ACS OMEGA

Article

http://pubs.acs.org/journal/acsodf

Hierarchical Self-Assembly of Noncanonical Guanine Nucleobases on Graphene

Nabanita Saikia,*[,†] Kevin Waters,[†] Shashi P. Karna,[‡] and Ravindra Pandey*[,†]

[†]Department of Physics, Michigan Technological University, 1400 Townsend Drive, Houghton, Michigan 49931, United States

[‡]Weapons and Materials Research Directorate, U.S. Army Research Laboratory, ATTN: RDRL-WM, Aberdeen Proving Ground, Aberdeen, Maryland 21005-5069, United States

Supporting Information

ABSTRACT: Self-assembly characterizes the fundamental basis toward realizing the formation of highly ordered hierarchical heterostructures. A systematic approach toward the supramolecular self-assembly of free-standing guanine nucleobases and the role of graphene as a substrate in directing the monolayer assembly are investigated using the molecular dynamics simulation. We find that the free-standing bases in gas phase aggregate into clusters dominated by intermolecular H-bonds, whereas in solvent, substantial screening of intermolecular interactions results in π-stacked configurations. Interestingly, graphene facilitates the monolayer assembly of the bases mediated through the base−substrate $\pi-\pi$ stacking. The bases assemble in a highly compact network in gas phase, whereas in solvent, a high degree of immobilization is attributed to the disruption of intermolecular interactions. Graphene-induced stabilization/aggregation of free-standing guanine bases appears as one of the prerequisites governing molecular ordering and assembly at the solid/liquid interface. The results demonstrate an interplay between intermolecular and π-stacking interactions, central to the molecular recognition, aggregation dynamics, and patterned growth of functional molecules on two-dimensional nanomaterials.

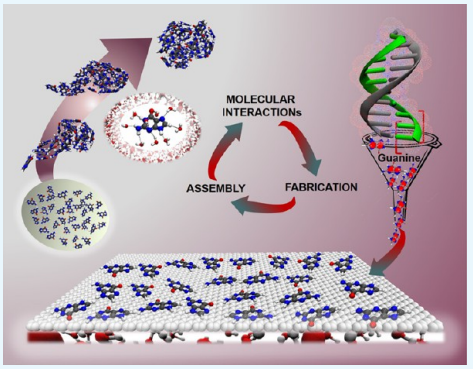

INTRODUCTION

Molecular self-assembly represents a "bottom-up" approach in controlling the growth and fabrication of biointegrated materials with the desired functionality within nanometer precision.[1,2] The self-assembly and molecular ordering from a random (disordered) to well-patterned (ordered) structure is paramount in the large-scale fabrication of three-dimensional structural motifs and hierarchical architectures.[3−5] Recent examples include self-assembled DNA motifs,[6] which find applications in DNA-based microarrays (i.e., DNA chips),[7] the detection of proteins involved in cell signaling (i.e., protein chips),[8] sensing for the rapid detection of functional molecules and pathogens, and biomolecular recognition at the solid/liquid interface.[9−11]

Of the four DNA nucleobases, guanine (G) has drawn considerable research interest over the past few years. The low ionization potential coupled with strong electron−donor characteristics[12] facilitates charge transport within G molecules.[13,14] In addition, three H-bond acceptor (N_7, N_3, and O_6) and two H-bond donor (N_1 and N_2) sites simultaneously behave as Brønsted acid and base and exhibit an exquisite internal H-bonded motif.[15] Also, G-rich moieties demonstrate a high propensity to fold into hierarchical motifs and self-assembled nanostructures like quadruplex (G4's),[16] honeycomb arrangements, nanowires,[17] and sheetlike structures.[18−20]

In general, the supramolecular self-assembly of functional molecules is mitigated in the presence of an inorganic substrate, which serves as a template for the growth. In most cases, an array of diverse polymorphic structures is observed and the efficacy of a molecule to a substrate governs the nature of the molecular orientation and assembly.[21,22] The self-assembly of DNA nucleobases and its derivatives on two-dimensional (2D) substrates like graphene,[23] highly ordered pyrolytic graphite (HOPG),[24−26] MoS_2,[25,27] hexagonal BN (h-BN),[28,29] Au (111),[30,31] and $SrTiO_3$ (100)[32] substrates has been reported.[33] Scanning tunneling microscopy imaging of the ordering of G nucleobases on MoS_2 reveals distinct isolated structureless blobs with parallel rows of alternating intermolecular H-bridge bonds.[28] An anisotropic patterned assembly of single- and double-stranded DNA on graphene nanoribbons (GNRs) was ascribed to the donor−acceptor interactions, wherein electric dipole and van der Waals (vdW) coupling facilitates the charge transfer between DNA and GNRs.[34] Atomic force microscopy (AFM) imaging of G molecules on freshly cleaved HOPG[35] showed that G molecules condense in small nuclei without the formation of an ordered assembly. Likewise, molecular packing of adenine on a (0001) graphite surface was found to be commensurate with the graphite surface.[36] In contrast to the preferential π-stacking on graphene, the ionic nature of the h-

Received: April 28, 2017
Accepted: June 27, 2017
Published: July 12, 2017

DOI: 10.1021/acsomega.7b00528
ACS Omega 2017, 2, 3457−3466

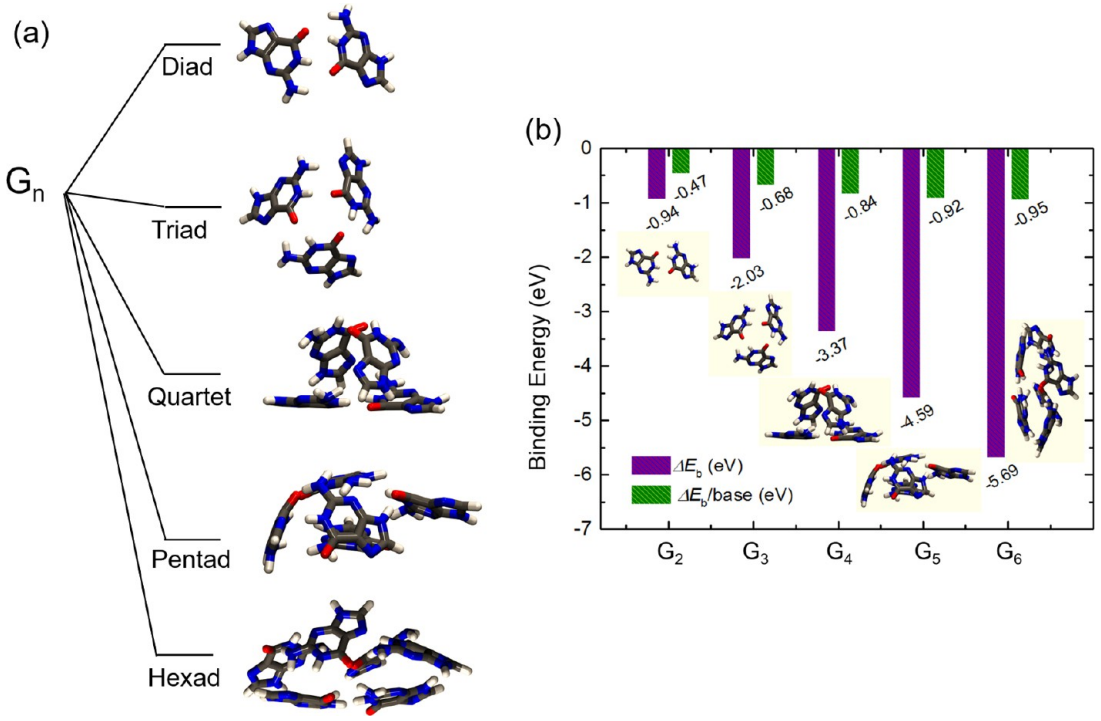

Figure 1. (a) Snapshots of G_n bases (for n = 2−6) and (b) binding energy and binding energy/base of G_n bases in the gas phase.

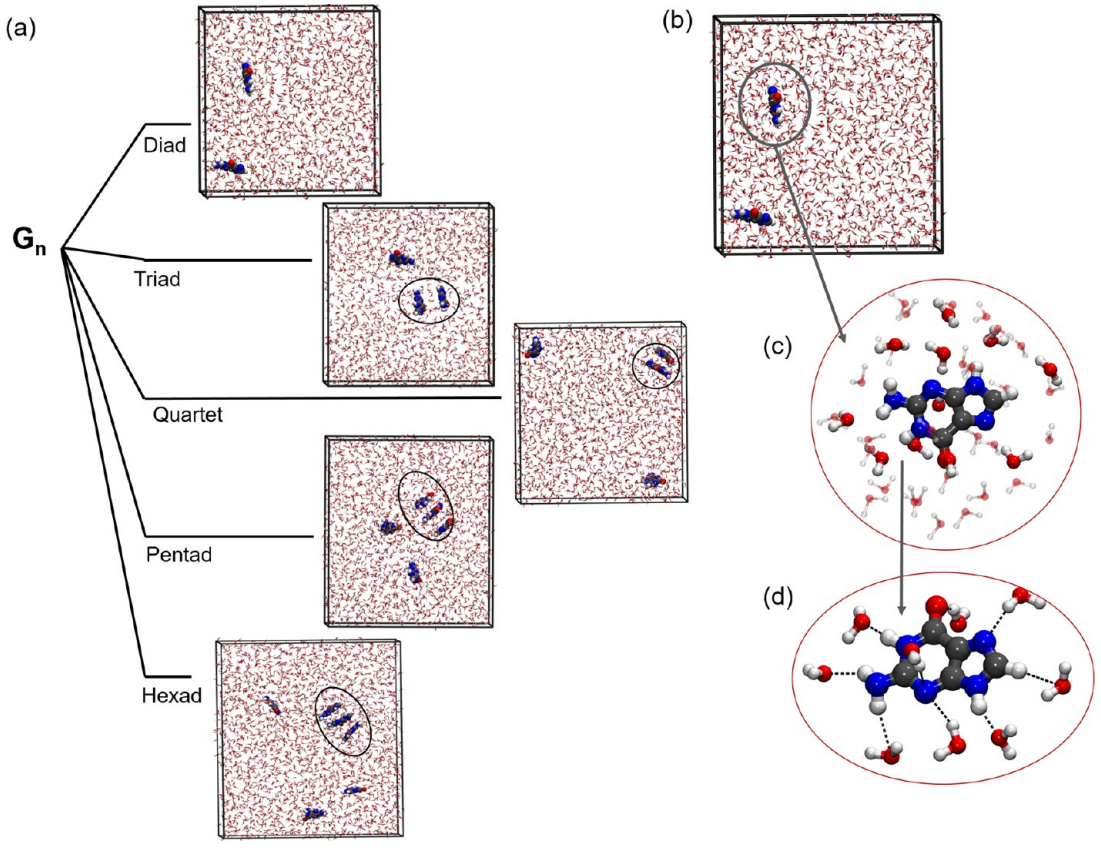

Figure 2. (a) Solvent-phase snapshots of G_n (for n = 2−6) bases, (b, c) water hydration sphere and ordering of water molecules along the guanine molecule, and (d) approximately nine water molecules constituting the first water hydration sphere.

BN sheet results in stronger bioconjugated complexes with high sensitivity toward the DNA/RNA nucleobases.[28,29]

Graphene is a versatile 2D nanomaterial and an ideal candidate for the fabrication of novel biointegrated structures,[37] due to its atomically flat surface together with unique physical,

DOI: 10.1021/acsomega.7b00528
ACS Omega 2017, 2, 3457−3466

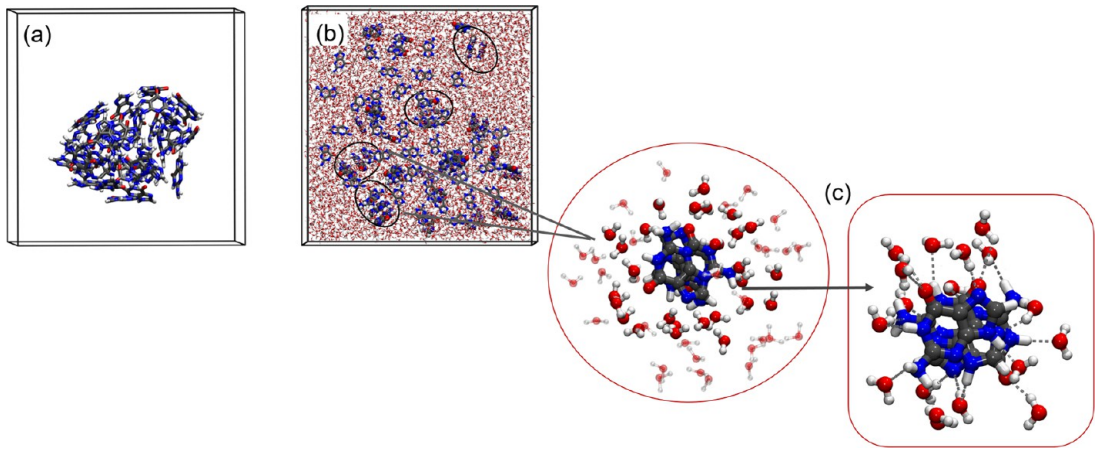

Figure 3. Snapshots of G_{36} bases in (a) gas phase and (b) solvent. (c) Schematic illustration of the water hydration sphere and ordering along the three stacked bases.

optical, and electronic properties. In our recent theoretical work based on the dispersion-corrected density functional theory (DFT-D2), we highlighted the role of graphene in stabilizing the physisorption of G_n bases.[38] We have demonstrated a substrate-induced structural transition in G_n bases and a preference of alignment over the stacked configurations on graphene. Realizing that first-principles calculations were limited to a small number of bases along with the fact that the solvation effect was treated via the implicit polarizable continuum model, we consider a larger set of G_n oligomers, thereby replicating the properties at longer length/time scales. Herein, with the help of molecular dynamics (MD) simulation, we investigate the self-assembly of free-standing noncanonical G_n nucleobases and the role of graphene in mediating the monolayer self-assembly of the bases as a function of the surface coverage. Specifically, our goal is to elucidate the crossover mechanism of base−base and base−substrate interactions that will help establish systematic pathways toward realizing molecular recognition and self-assembly under the given physiological conditions.

RESULTS AND DISCUSSION

Self-Assembly of G_n Bases with n = 2−6. Figure 1 depicts the snapshots of free-standing G_n bases in the gas phase. Conformational flexibility and the availability of donor/acceptor sites within the G base facilitate multiple modes of interaction, wherein the bases tend to aggregate, stabilized predominantly by intermolecular H-bonds, as shown in Figure 1a. The diad configuration is predicted to be nonplanar, whereas the triad configuration stabilizes in a semicage-like structure through bifurcated and intermolecular H-bonds. The quartet, pentad, and hexad configurations are stabilized via intermolecular H-bonds, and an increase in the number of homomers leads to aggregation (clustering) of the bases. The calculated binding energy, defined as the difference in the potential energy between the system and the constituents, increases with the number of bases, although the binding energy/base attains saturation from G_4 onward, suggesting a net stabilization of G_n complexes (Figure 1b).

The snapshots of free-standing G_n bases in solvent (Figure 2a) illustrate a disruption of intermolecular H-bonds within the base pairs; in the diad configuration, the bases are randomly dispersed with no preference for dimerization. With an increase in the number of bases, noncovalent π−π interactions lead to the stacked configurations, as highlighted by the black circles in Figure 2a, via the formation of a water hydration sphere around the bases. A close observation of the arrangement of water molecules around a guanine suggests a uniform ordering of water dipoles, and a maximum of nine water molecules constitute the first hydration sphere (Figure 2c,d) at an average H-bond distance of ∼1.90 Å. As water is a polar molecule with a high dielectric constant of 79.36, it introduces electrostatic screening of H-bonded interactions between the bases, thereby leading to the preference for π stacking in the solvent.

The number of H-bonds further supports the extent of H-bonded interactions stabilizing the G_n complexes in gas and solvent phases. The diad configuration is stabilized by two H-bonds (Figure S1, shown in green), as also predicted by the dispersion-corrected DFT results.[38] With an increase in the number of bases, the H-bond count increases to a maximum of seven for the hexad configuration in the gas phase, whereas the disruption of the intermolecular H-bond is substantiated in the solvent (Figure S1, shown in red). In gas phase, the average intermolecular H-bond distance is calculated to be <2.0 Å (Figure S2), although a fluctuation in the intermolecular H-bond distance is observed for the triad configuration. The root-mean-square deviation (RMSD) demonstrates significant fluctuation over the trajectory in the solvent compared to that in the gas phase (Figure S3) and can be accounted to the conformational variations within the G_n complexes (average RMSD is calculated to be <1.5 Å).

To provide a detailed understanding on the nature of molecular aggregation and self-assembly of free-standing G_n bases, we extended the simulation to larger G_n bases, namely, G_{12} and G_{36}, as discussed in the following section.

Self-Assembly of G_{12} and G_{36} Bases. In the gas phase, the free-standing G_{12} bases aggregate in a cagelike structure stabilized by intermolecular H-bonds along the outer cage and π stacking along the core, as depicted in Figure S4a. It is important to note that approximately nine G bases constitute the intermolecular H-bonded network within the cage structure (Figure S4b). The average binding energy and binding energy/base for G_{12} in the gas phase are calculated to be −13.2 and −1.1 eV, respectively. In the solvent, the preference for π−π stacking between the bases with a disruption of intermolecular H-bonds is highlighted (Figure S4c).

The RMSD suggests an overall stability of the G_{12} configuration, with the normalized RMSD values of ∼2.2 and

DOI: 10.1021/acsomega.7b00528
ACS Omega 2017, 2, 3457−3466

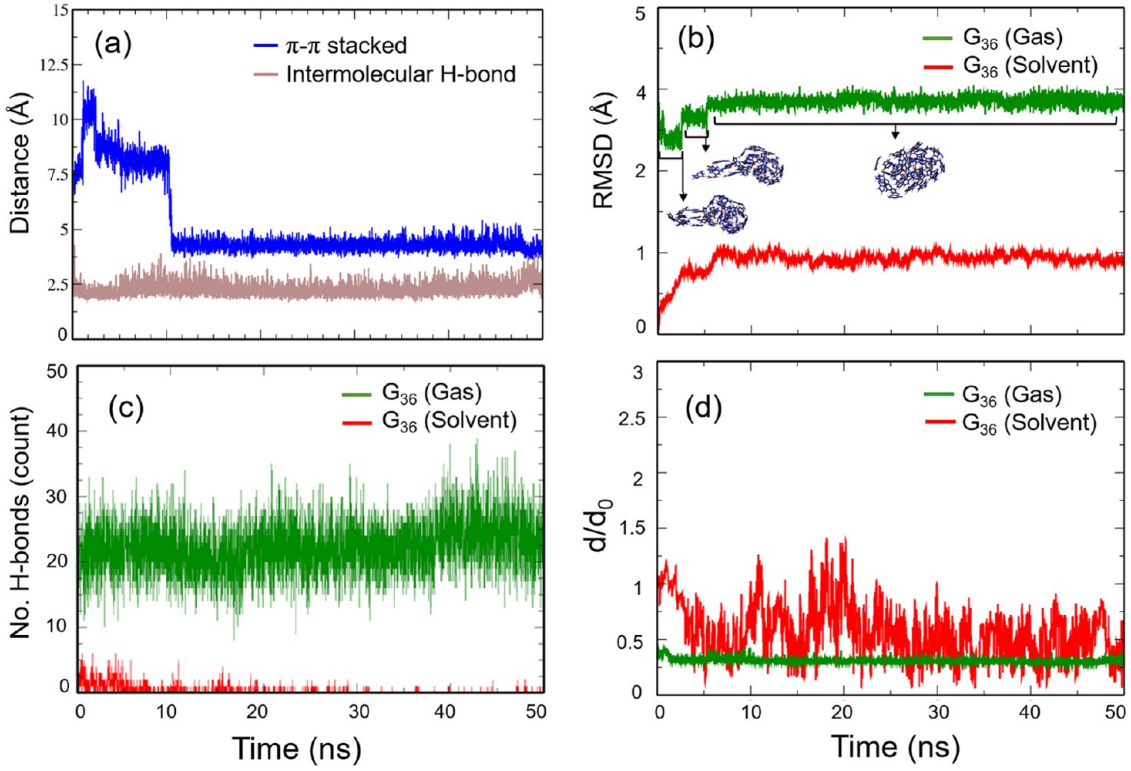

Figure 4. Evolution of the (a) $\pi-\pi$ stacked and intermolecular H-bond distances in gas phase, (b) normalized RMSD, (c) number of H-bonds, and (d) normalized center of mass (COM) distance of G_{36} bases in gas and solvent phases.

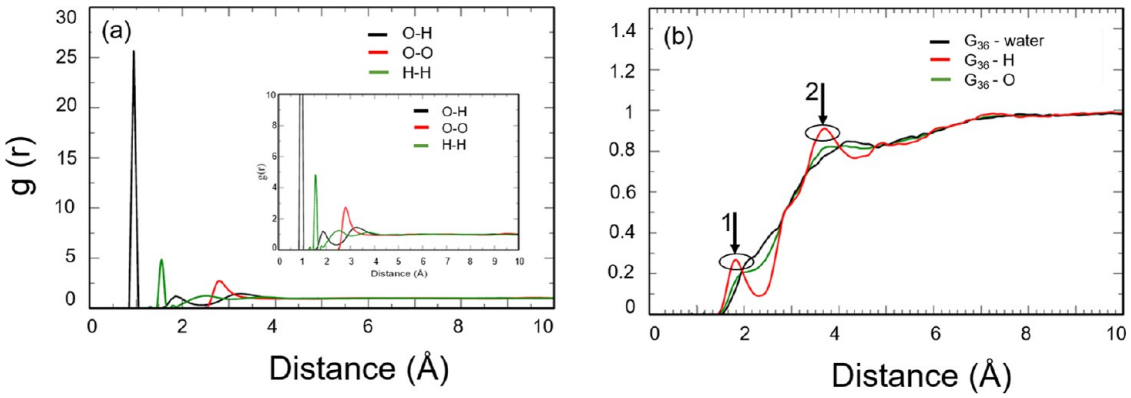

Figure 5. (a) RDF of O−H, O−O, and H−H bonds associated with the water molecules solvating G_{36} complex. (b) RDF of free-standing G_{36} bases in solvent.

~1.3 Å in the gas phase and the solvent, respectively (Figure S5a). In the solvent, fluctuations in RMSD over the trajectory are attributed to the random orientations and disruption of intermolecular interactions between the G_{12} bases. Similar to the trends observed in Figure 1, self-assembly of G_{12} leads to an increased H-bond count (average of ~12 H-bonds in the gas phase), whereas in the solvent, the disruption of intermolecular H-bonds leads to a reduced H-bond count of 1−2 (Figure S5b).

The radial distribution function (RDF) serves as a valuable tool to compute the nearest neighbors and the formation of water hydration spheres around G bases. The RDF between the oxygen atom of water molecules and the G base (red spline) depicts two characteristic peaks, one below 2.0 Å (peak 1) and the other close to 4.0 Å (peak 2), corresponding to the two ordered water hydration spheres. In the total RDF (green spline), contributions from the H-atom (black spline) overlay with the combined system (Figure S5c).

Likewise, the G_{36} bases aggregate in a highly compact network like G_{12}, stabilized via $\pi-\pi$ stacking along the core and intermolecular H-bonds along the outer cage in the gas phase (Figure 3a). We find that an increase in the number of bases facilitates an enhanced interaction within the complex, with binding energy and binding energy/base of −46.65 and −1.30 eV, respectively. In the solvent, screening of the intermolecular interactions leads to the formation of distinct $\pi-\pi$ stacked domains (black circles in Figure 3b) and ~17 water molecules constitute the water hydration sphere around the stacked bases (Figure 3c).

To substantiate the two modes of noncovalent interaction stabilizing the G_{36} configuration, we compared the dynamic evolution of $\pi-\pi$ and intermolecular H-bond distances, as

DOI: 10.1021/acsomega.7b00528
ACS Omega 2017, 2, 3457−3466

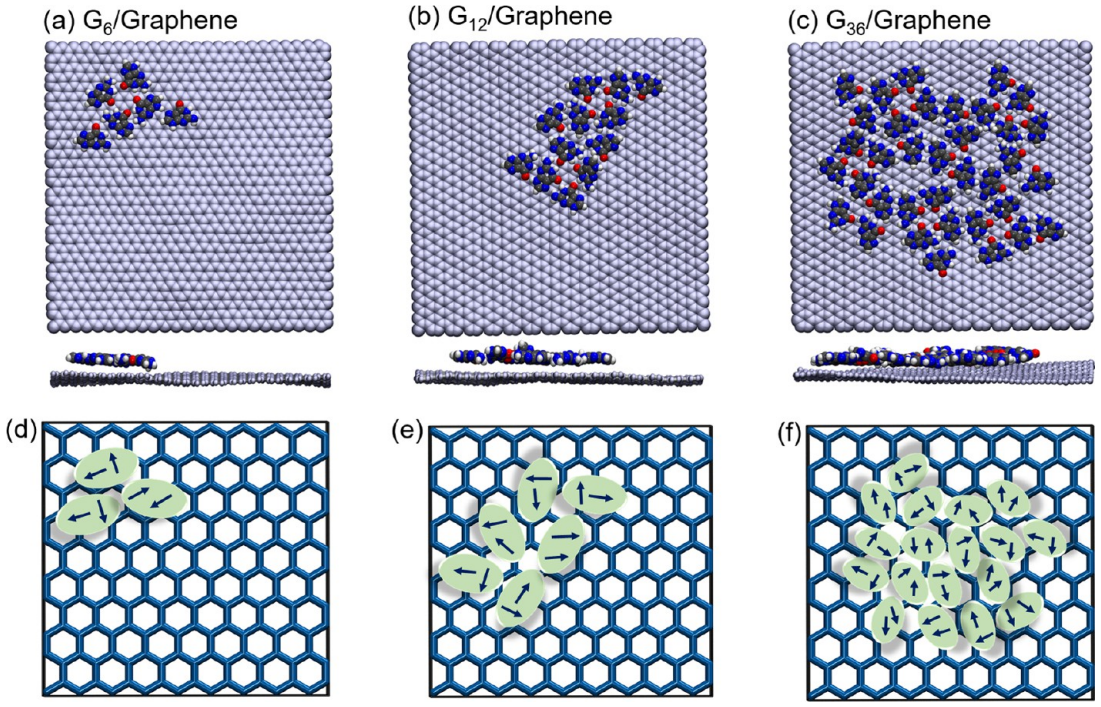

Figure 6. (a–c) Snapshots of G_n bases (n = 6, 12, and 36) adsorbed on graphene monolayer in gas phase. (d–f) Dipole alignment of G molecules.

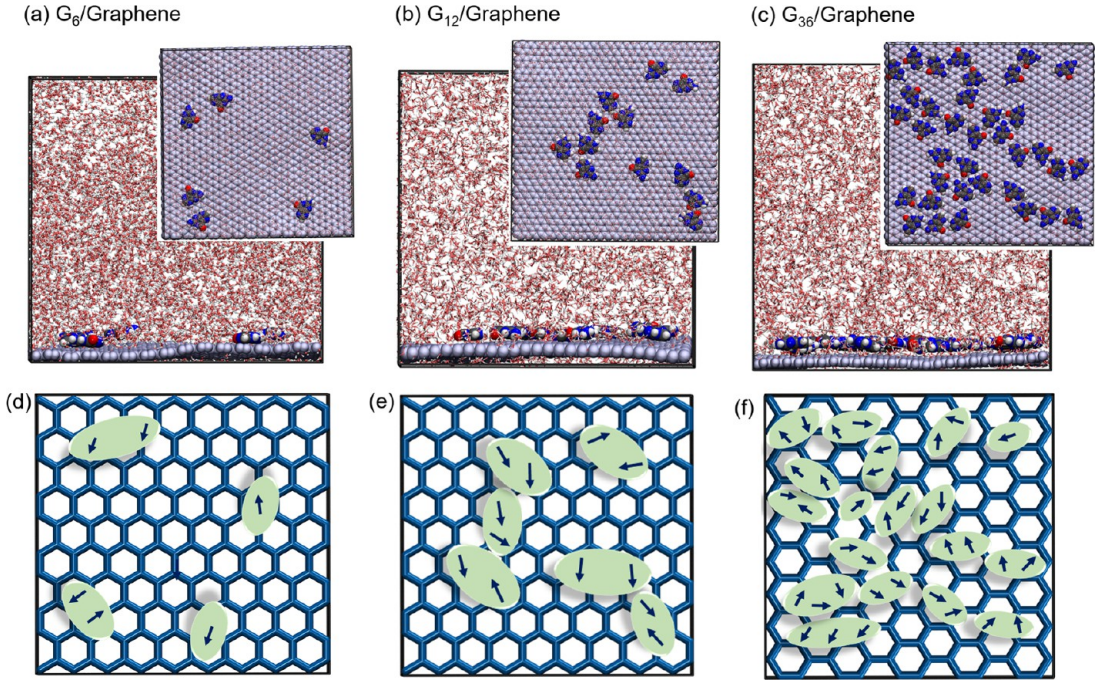

Figure 7. (a–c) Snapshots of G_n bases (n = 6, 12, and 36) physisorbed on graphene in solvent. (d–f) Dipole alignment of G molecules.

illustrated in Figure 4a. The average π-stacking distance between the base pairs is calculated to be approximately 3.5–4.0 Å. It is important to note that for the first 10 ns, no π stacking between the bases was realized (Figure 4a, shown in blue), as most of the bases that have aggregated are stabilized by an intermolecular H-bonded network. The average intermolecular H-bond distance is <2.5 Å, which falls within the intermolecular H-bond regime. The results agree with our previously reported dispersion-corrected DFT-D2 calculations, where the average intermolecular H-bond distance in G_n bases was calculated to be approximately 1.8–1.9 Å.[38]

The evolution in the structure and conformational stability of G_{36} bases can be considered from the analysis of the normalized RMSD over the trajectory, as depicted in Figure 4b. In the gas phase, the two break points around 5 and 10 ns (shown in green) are correlated to the change in the configuration, in which the tail portion of G_{36} assembles to a completely globular network beyond 10 ns. The RMSD in the solvent increases in the beginning and then saturates around ∼1.0 Å, suggesting an

DOI: 10.1021/acsomega.7b00528
ACS Omega 2017, 2, 3457–3466

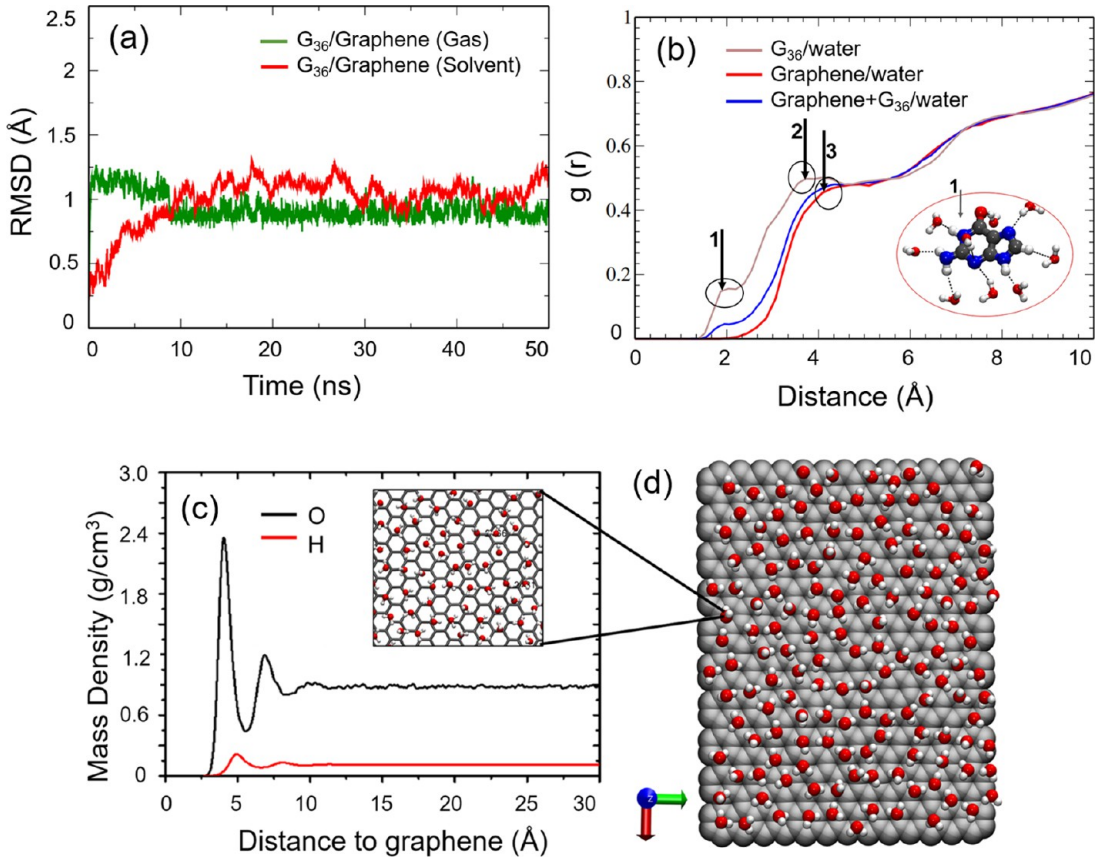

Figure 8. (a) Normalized RMSD for G_{36}/graphene in gas (green) and solvent (red) phases, (b) RDF of G_{36}/graphene and the constituents in solvent, (c) mass density profile of water molecules along graphene, and (d) extrapolation of the inset in (c) depicting a cross section of the orientation of water molecules on graphene.

overall stability of the system. The average H-bond count of ∼23 in the gas phase reduces to ∼2 in the solvent, which substantiates to the substantial screening of intermolecular bonds by water molecules (Figure 4c). In the gas phase, the normalized COM remains nearly constant at ∼0.35, with no structural variation (Figure 4d), whereas in the solvent, substantial fluctuations in the COM is attributed to the random dispersion of the bases.

Figure 5a illustrates the pairwise RDF of O−H, O−O, and H−H bonds in water molecules, and the inset depicts the RDF profile of water simulation in the absence of G molecules. The corresponding RDF of the solvated system is shown in Figure 5b, wherein the RDF of the O−H bond at 1.0 Å corresponds to the calculated O−H bond length in water. Likewise, the H−H (O−O) bond length is calculated to be 1.6 (2.75) Å, which is in excellent agreement with the reported RDF of TIP3P water using the CHARMM force field.[39] In the combined system (Figure 5b), the RDF of the oxygen atom of G bases depicts two characteristic peaks, one at ∼1.8 Å (peak 1) and the other close to 4.0 Å (peak 2), which correspond to the two ordered hydration spheres. The H-atom contributions to the total RDF overlays with the combined system (black spline). The RDF of G_{36} in the gas and solvent phases is provided in Figure S6a,b.

Self-Assembly of G_n Bases on Graphene with n = 6, 12, and 36. The dynamics of G_n bases in the presence of graphene was considered to elucidate the role of the substrate in regulating the monolayer assembly, as the free-standing bases prefer to aggregate (cluster) rather than form a self-assembled monolayer. The snapshots of G_n/graphene complexes (for n = 6, 12, and 36) in the gas phase demonstrate the monolayer assembly on graphene, stabilized primarily by the base−base intermolecular H-bonds and base−graphene π-stacking interactions (Figure 6a−c). At a low surface coverage (i.e., for n = 6 and 12), the bases are aligned in a linear array, whereas at a high surface coverage (i.e., n = 36), the bases aggregate in a highly condensed network with no well-defined patterned array. The polar nature of G molecules coupled with the possibility of interaction via donor/acceptor sites facilitates myriad polymorphic arrangements within the complex, as described by the arrow notation corresponding to the dipole orientation in Figure 6d−f. Notably, we observed the G-quartet domains within the base alignment, as illustrated in the top images of Figure 6a−c.

In the solvent, screening of the intermolecular bonds by water molecules leads to a high degree of immobilization of the bases on graphene (Figure 7a). With an increase in the number of physisorbed bases, aggregation leads to base dimerization, overcoming the base−water dipolar interactions, and the base−substrate π−π stacking predominates the base−base intermolecular interactions (Figure 7b). The interplanar distance between graphene and G_n bases is calculated to be ∼3.4 Å, which agrees with the reported π-stacking distance of aromatic molecules adsorbed on graphene.[40,41] For the G_{36}/graphene complex (Figure 7c), an increase in the number of homomers facilitates intermolecular H-bonded interactions along graphene. Given the fact that G bases can exhibit multiple interacting modes facilitated by the acceptor−donor sites along with the competing steric hindrance induced by the water

DOI: 10.1021/acsomega.7b00528
ACS Omega 2017, 2, 3457−3466

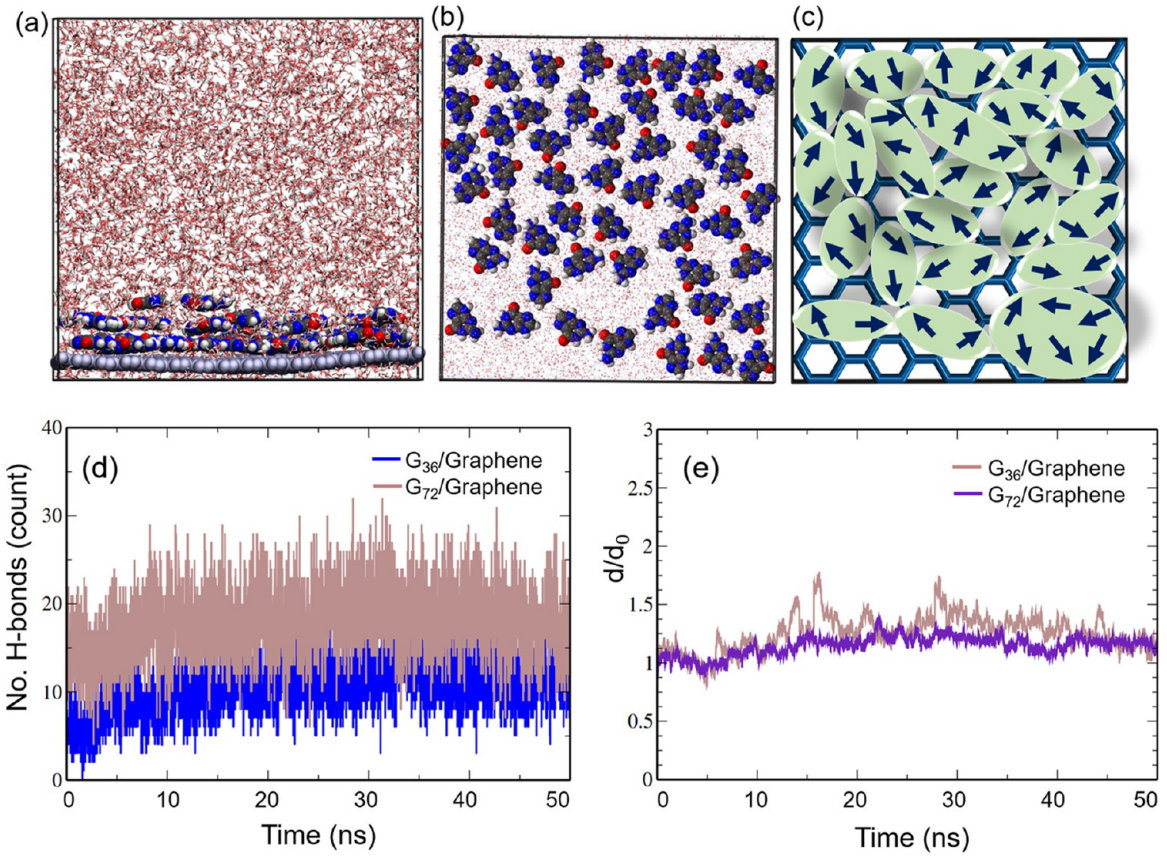

Figure 9. Snapshots of G_{72}/graphene in solvent: (a) side view, (b) front view, and (c) dipole alignment of the G bases. (d) Number of H-bonds and (e) normalized COM between graphene and G bases in G_{36}/graphene and G_{72}/graphene complexes.

molecules, random dispersions were observed with a reduced affinity between the bases, especially at a low surface coverage.

The interaction energy of G_n/graphene complexes together with variations in the corresponding vdW and electrostatic energies is depicted in Figure S7a–c. For a single guanine nucleobase adsorbed on graphene, the interaction energies in the gas and solvent phases are calculated to be −0.25 and −0.77 eV, respectively. The free-standing G_n bases in the gas phase have a comparatively higher interaction energy than the bases adsorbed on graphene. At the level of dispersion-corrected DFT, a similar trend in the interaction energy was predicted for free-standing and graphene-supported G_n bases. With an increase in the number of bases physisorbed on graphene, the interaction energy is calculated to be about −0.5 eV in the gas phase, whereas in the solvent, it increases to about −7.0 to −11.3 eV, which may be attributed to the water molecules stabilizing the adsorption of G_n complexes on graphene and favors base−base dimerization over base−base aggregation into clusters in the gas phase. Thus, graphene facilitates the monolayer dispersion of the G_n bases in the gas and solvent phases, as opposed to the self-aggregation of free-standing bases in the gas phase and π-stacked domains in the solvent. The vdW energy increases as a function of the surface coverage (Figure S7b) due to the increase in the $\pi-\pi$ stacking interactions with an increase in the number of molecules. On the other hand, the electrostatic energy decreases with an increase in the surface coverage (Figure S7c), suggesting an enhanced intermolecular H-bonded interaction and a net weakening of the electrostatic interactions between the G_n bases at a high surface coverage. The base−base stacking interaction energy and the base−substrate interaction energy have been investigated at the level of DFT[42,43,38] and ab initio MD simulation.[44] At the level of dispersion-corrected DFT,[38] we have discussed that in the presence of explicit waters base−base stacking is energetically favored over the aligned configuration, with more water molecules solvating the bases with the formation of water hydration spheres in the former configuration. This implied that graphene helps to disperse the guanine bases and favors the monolayer-aligned configuration over the stacked mode of adsorption.

The normalized RMSD values for G_6/graphene and G_{12}/graphene in the gas and solvent phases were further compared, as depicted in Figure S8. In the gas phase, the RMSD of G_{12}/graphene shows a break at ∼38 ns, which is associated with the reorientation of G_{12} on graphene, as shown in the adjoining schematic of Figure S8b. In the solvent, the average RMSD is calculated to be <1.5 Å, and screening of the intermolecular interactions by water molecules results in random fluctuations over the trajectory. The average RMSD of G_{36}/graphene at <1.0 Å (Figure 8a) suggests a higher degree of stability introduced by graphene, signifying the substrate-induced self-assembly of the bases at a high surface coverage. For free-standing G_{36} bases and in G_{36}/graphene in the solvent phase, the normalized RMSD of about 1 Å suggests that the base−base self-aggregation in free standing is likely in the solvent phase for a higher number of bases and that the bases assume to aggregate in stacked configurations. In the presence of graphene, monolayer adsorption of the G_{36} bases facilitates the base−base aggregation in an aligned configuration on graphene, whereas, at a highly saturated base coverage, the base−base

DOI: 10.1021/acsomega.7b00528
ACS Omega 2017, 2, 3457−3466

aggregation is mediated via both aligned and stacked configurations.

The number of H-bonds in the G_n/graphene complex increases with an increase in the number of physisorbed bases, as shown in Figure S10. Relative to the cases of free-standing G_n bases (Figures 1 and 2), the increase in the H-bond count suggests that the incorporation of graphene facilitates the base aggregation in both gas and solvent phases. For example, the presence of graphene leads to an increased H-bond count, with an average of ∼5 and ∼10 H-bonds for G_{12}/graphene and G_{36}/graphene, respectively, compared to an average of 1−2 H-bonds for the free-standing counterparts. The simulation results thereby suggest a correlation of the extent of surface coverage density on the overall stability and self-assembly/aggregation of G_n bases on graphene.

High Surface Coverage of G Bases on Graphene: G_{72}/Graphene. The high surface coverage simulated with 72 bases was considered to provide additional insights into the competitive interactions that govern the self-assembly process. It is important to note that, at a highly saturated surface coverage, molecular and steric constraints in the packing of G polymorphs render stacking patterns between the bases in addition to the aligned configurations, as illustrated in the snapshot in Figure 9a. We find that ∼48 bases can fully saturate the graphene surface, as depicted in Figure 9b, and apart from the monolayer assembly, π stacking between the bases is observed for the bases not in close proximity of graphene. An enhanced H-bond stabilization is observed with an average of ∼18 H-bonds between the bases (Figure 9d). The RMSD of G_{72}/graphene suggests an overall stability of the system in the solvent at an average value below 1.25 Å, as depicted in Figure S11a. The average H-bond distance between the bases is calculated to be ∼2.0 Å, which correlates well with the intermolecular H-bond distance in free-standing G_n bases, whereas the π-stacked distance between the base and the substrate is ∼3.55 Å (Figure S11b).

A comparison of the normalized COM in the G_{36}/graphene and G_{72}/graphene complexes is shown in Figure 9e. The fluctuations in G_{36}/graphene at an average value of 1.25 can be attributed to the conformational flexibility in orientations of guanine bases physisorbed on graphene. On the other hand, a highly saturated surface corresponding to G_{72}/graphene exhibits a nearly constant COM throughout the trajectory at around 1.0. This is because an almost complete surface coverage of graphene restrains the free rattling of the physisorbed bases. Relative to a high degree of fluctuations in COM for free-standing G_n bases (Figure 4d), the presence of a graphene substrate also mitigates base−base intermolecular interactions, thereby stabilizing the molecular assembly, especially at a high surface coverage in the solvent.

To understand the energetics of the base−base stacking interaction and the base−substrate interaction for G_n/graphene, calculations were using the vdW dispersion-corrected DFT.[38] In these calculations, G_2 base was taken to represent the case of a lower surface coverage on graphene. The gas-phase interaction energies of the stacked and aligned G_2 bases on graphene were calculated to be −1.04 and −1.72 eV, respectively. The DFT results therefore suggest preference for the aligned base configurations on graphene, wherein the aligned geometries facilitate a maximum π-orbital overlap associated with the interacting moieties. It is important to note that the gas-phase interaction energies of the free-standing G_2 bases in the stacked and aligned configurations are calculated to be −1.01 and 1.48 eV, respectively. The MD results are therefore in agreement with the DFT results for the low surface coverage of the bases on graphene.

The preference of G_n bases to assimilate in disordered aggregates with no well-defined arrays on the monolayer graphene agrees with previous AFM studies of G_n bases adsorbed on HOPG in the presence of water solvent media at high and fully saturated surface coverages.[35] The preference of the bases to assimilate in disordered aggregates on the monolayer graphene is also in agreement with the observed stacked polymeric arrays of G bases on the underlying Au(111) substrate.[45,46] Our simulation results predict distinctive trends under ultrahigh vacuum conditions and in water solvent media, suggesting that the solvent polarity (polar vs nonpolar) contributing to the dipolar interactions between water/G bases and water molecules renders conformational flexibility toward the assembly process. Free-standing graphene with its inherent rippling characteristics determines the nature of the assembly and flexibility of G bases to adopt various polymorphs and packing structures, as opposed to forming perfectly aligned arrays on the HOPG substrate. Although graphene mitigates the monolayer assembly of G bases, the formation of disordered aggregates especially in solvent phase can be described as a collective noncovalent interaction of intermolecular H-bond, $\pi-\pi$ stacking, cooperative, and hydrophobic interactions in predicting the molecular stability and self-assembly at the solid/liquid interface.

SUMMARY

The self-assembly of free-standing and graphene-supported noncanonical G_n nucleobases is investigated by employing the MD simulation method. We find that the molecular aggregation and self-assembly are governed by the interplay of the base−base and base−substrate interactions. The base−substrate interactions mainly determine the formation of the self-assembled monolayer on graphene, whereas the base−base interactions govern the nature of aggregation of the free-standing G molecules.

In the gas phase, the free-standing G_n bases prefer to aggregate, stabilized by intermolecular H-bond and π-stacking interactions along the core. In the solvent, the stacking mode is preferred due to screening of the intermolecular interactions. The substrate-induced effect is substantial in driving the monolayer assembly, thereby regulating the growth and stabilization of the bases. The G_n bases adopt random dispersion on graphene, rendered from the inherent polarity and the availability of donor/acceptor sites facilitating myriad polymorphic arrangements. In the solvent, a high degree of immobilization of the bases on graphene occurs at a low surface coverage. On the other hand, at a high surface coverage, steric constraints in the packing of G_n polymorphs render stacking patterns between the bases in addition to the monolayer coverage, competing with the water molecules toward the self-assembly on graphene. In the solvent, the preference of G_n bases to assimilate in disordered aggregates with no well-defined arrays on graphene agrees well with previous AFM studies of G_n bases adsorbed on HOPG. The calculated results help provide a comprehensive yet succinct understanding of the dominant interactions governing the self-assembly of free-standing noncanonical G_n nucleobases and the role of the 2D material substrate toward realizing self-assembled hierarchical structural motifs. The future direction which we foresee is the application of the assembled heterostructures as templates for

DOI: 10.1021/acsomega.7b00528
ACS Omega 2017, 2, 3457−3466

the growth and fabrication of DNA-based sensors, sequencing of DNA oligonucleotides, translocation through nanopores, and in DNA-based nanoelectronic devices.

COMPUTATIONAL DETAILS

The MD simulations were performed using the isothermal−isobaric (NPT) and NVT ensembles in both gas (vacuum) and solvent phases using the NAMD code.[47] The all-atom CHARMM27 force field[48] was employed for graphene, which includes bonded and nonbonded parameters.[49] The simulations were performed at room temperature (298.15 K) using the Langevin dynamics, and the Langevin piston Nosé−Hoover method was employed to maintain the pressure at 101.3 kPa. The particle mesh Ewald[50] summation was used to calculate the periodic electrostatic interactions with a long-range cutoff of 12.0 Å. For the solvent phase, the water molecules were represented by the TIP3P water, with constraints applied to the bond lengths and angles of the water molecules using the SETTLE algorithm. Except for the water molecules, all other atoms were relaxed during the simulation to capture the dynamics of interaction.

The free-standing G_n bases (for n = 2−6, 12, and 36) were simulated in a periodic supercell of (50 × 50 × 50) Å^3. Calculations incorporated 2000 steps of energy minimization using the conjugate gradient algorithm, followed by 1.5 ns of production run in the gas and solvent phases using the NVT and NPT ensembles, respectively. For larger G_n homomers (i.e., n = 12 and 36), we proceeded with 50 ns of the production run in the gas and solvent phases, with the other variables remaining unchanged, to have a detailed understanding on the dynamic evolution of molecular complexes. It has been previously established that MD simulations with time scales of ∼50 ns are sufficient to attain stable molecular complexes for similar systems in both gas and solvent phases.[51]

The graphene sheet was constructed in a periodic supercell having a dimension of (61.6 × 62.4) Å^2 comprising 1500 carbon atoms. The MD simulation of the G_n/graphene complex incorporated 2000 steps of energy minimization, followed by 50 ns of production run at a timestep of 1.0 fs. In the solvent, we also performed simulated annealing with a gradual increment of temperature from 298 to 700 K at an interval of 50 K and quenching the complex to 298 K with a decrement interval of 50 K. To determine the preferred orientation of the adsorption of G bases on graphene, we considered both parallel and perpendicular orientations of the adsorption. Quite interestingly, the G_n bases that were initially aligned perpendicular at ∼7 Å away from the graphene basal plane reverted to a parallel stacked configuration within 1 ns of the simulation, suggesting the preference for interaction via a parallel stacked mode.

The convergence of the simulation in terms of the measure of the variation of the average distance between the atoms was examined by analyzing the RMSD over the trajectory. For the last 1 ns of the 50 ns trajectory, additional components of the analysis, namely, the RDF, normalized COM distance between the G_n bases, G_n/graphene, and water density profile, were calculated. The RMSD is an indicator of the overall stability of the system over the trajectory, and a uniform RMSD suggests no major fluctuations in the system. The RDF or the pair correlation function denoted by $g(r)$ represents the correlation between atom pairs or the probability to find an atom at a distance r from another atom chosen as the reference. At short distances (less than atomic diameter), the value of $g(r)$ is zero, which corresponds to the strong repulsive forces. The first large peak demonstrates the likeliness of two molecules to be found at this separation. At long distances, $g(r)$ approaches the value of one, which indicates that there is no long-range order. The number of H-bonds was calculated with the help of the VMD[52] plugin over the trajectory between the G_n bases. The number of H-bonds provides a qualitative estimate of the average number of H-bonds stabilizing the G_n configurations in the gas and solvent phases. The normalized RMSD, RDF, and COM plots were obtained using the VMD plugin. GaussView within the Gaussian09 suite of programs and VMD were utilized to construct the initial configurations of G_n bases, graphene, and G_n/graphene complexes.

The interaction energy of the G_n/graphene complex was calculated using a two-box method, given by

$$E_{int} = E_{close} - E_{away} \quad (1)$$

where E_{close} and E_{away} are the potential energies corresponding to the configurations of G_n/graphene when G_n molecules are close and away from graphene surface, respectively. The away configuration mimics an isolated system, where G_n bases are about ∼30 Å separated from graphene.

ASSOCIATED CONTENT

Supporting Information

The Supporting Information is available free of charge on the ACS Publications website at DOI: 10.1021/acsomega.7b00528.

The number of H-bonds, intermolecular H-bond distance, RMSD of free-standing G_n bases in gas and solvent phases; RDF of G_{36} bases in gas and solvent phases, number of H-bonds for the G_n/graphene complex and RDF of the G_6/graphene and G_{12}/graphene complexes; interaction energy of the G_n/graphene complexes, and time evolution of vdW and electrostatic energies of G_n adsorbed on graphene as a function of the surface coverage in solvent phase; RMSD for G_6/graphene and G_{12}/graphene complexes and the number of H-bonds for the G_n/graphene complex in gas and solvent phases (PDF)

AUTHOR INFORMATION

Corresponding Authors

*E-mail: nsaikia@mtu.edu (N.S.).
*E-mail: pandey@mtu.edu (R.P.).

ORCID

Nabanita Saikia: 0000-0001-9648-2363
Kevin Waters: 0000-0003-3828-8647

Notes

The authors declare no competing financial interest.

ACKNOWLEDGMENTS

The authors are grateful to Prof. Max Seel and Dr. S. Gowtham of Michigan Technological University for their insightful advice, suggestions, and helpful discussions. N.S. acknowledges financial support from Michigan Technological University, Houghton, MI. Computational resources at Michigan Technological University with SUPERIOR high-performance computing cluster were utilized. The research was partially supported by the Army Research Office (ARO) through grant number W911NF-14-2-0088.

DOI: 10.1021/acsomega.7b00528
ACS Omega 2017, 2, 3457−3466

REFERENCES

(1) Michl, J.; Magnera, T. F. *Proc. Natl. Acad. Sci. U.S.A.* **2002**, *99*, 4788−4792.
(2) Winfree, E.; Liu, F.; Wenzler, L. A.; Seeman, N. C. *Nature* **1998**, *394*, 539−544.
(3) Lehn, J.-M. *Supramolecular Chemistry: Concepts and Perspectives*; VCH-Wiley: Weinheim, 1995; pp 255−266.
(4) Otero, R.; Gallero, J. M.; Vazquez de Parga, A. L.; Martin, N.; Miranda, R. *Adv. Mater.* **2011**, *23*, 5148−5176.
(5) Kumar, A.; Banerjee, K.; Liljeroth, P. *Nanotechnology* **2017**, *28*, No. 082001.
(6) Kasemo, B. *Surf. Sci.* **2002**, *500*, 656−677.
(7) Hoheisel, J. D. *Nat. Rev. Genet.* **2006**, *7*, 200−210.
(8) Zhu, H.; Bilgin, M.; Bangham, R.; Hall, D.; Casamayor, A.; Bertone, P.; Lan, N.; Jansen, R.; Bidlingmaier, S.; Houfek, T.; Mitchell, T.; Miller, P.; Dean, R. A.; Gerstein, M.; Snyder, M. *Science* **2001**, *293*, 2101−2105.
(9) Soper, S. A.; Brown, K.; Ellington, A.; Frazier, B.; Garcia- Manero, G.; Gau, V.; Gutman, S. I.; Hayes, D. F.; Korte, B.; Landers, J. L.; Larson, D.; Ligler, F.; Majumdar, A.; Mascini, M.; Nolte, D.; Rosenzweig, Z.; Wang, J.; Wilson, D. *Biosens. Bioelectron.* **2006**, *21*, 1932−1942.
(10) Liu, X.; Zheng, F.; Jürgensen, A.; Perez-Dieste, V.; Petrovykh, D. Y.; Abbott, N. L.; Himpsel, F. J. *Can. J. Chem.* **2007**, *85*, 793−800.
(11) Zhao, W.-W.; Xu, J.-J.; Chen, H.-Y. *Chem. Rev.* **2014**, *114*, 7421−7441.
(12) Seidel, C. A. M.; Schulz, A.; Sauer, M. H. M. *J. Phys. Chem.* **1996**, *100*, 5541−5553.
(13) Preuss, M.; Schmidt, W. G.; Seino, K.; Furthmuller, J.; Bechstedt, F. *J. Comput. Chem.* **2004**, *25*, 112−122.
(14) Wetmore, S. D.; Boyd, R. J.; Eriksson, L. A. *Chem. Phys. Lett.* **2000**, *322*, 129−135.
(15) Dawson, R. M. C.; Elliot, W. H.; Jones, K. M. *Data for Biochemical Research*, 3rd ed.; Clarendon Press: Oxford, U.K., 1986; pp 87−97.
(16) Hastie, N. D.; Dempster, M.; Dunlop, M.; Thompson, A.; Green, D.; Allshire, R. *Nature* **1990**, *346*, 866−868.
(17) Borovok, N.; Molotsky, T.; Ghabboun, J.; Porath, D.; Kotlyar, A. *Anal. Biochem.* **2008**, *374*, 71−78.
(18) Li, Y.; Dong, M.; Otzen, D. E.; Yao, Y.; Liu, B.; Besenbacher, F.; Mamdouh, W. *Langmuir* **2009**, *25*, 13432−13437.
(19) Tao, N. J.; Derose, J. A.; Lindsay, S. M. *J. Phys. Chem.* **1993**, *97*, 910−919.
(20) Yoshikawa, I.; Sawayama, J.; Araki, K. *Angew. Chem., Int. Ed.* **2008**, *47*, 1038−1041.
(21) Ciesielski, A.; Samori, P. *Adv. Mater.* **2016**, *28*, 6030−6051.
(22) Liu, L.; Xia, D.; Klausen, L. H.; Dong, M. *Int. J. Mol. Sci.* **2014**, *15*, 1901−1914.
(23) Ahmed, T.; Kilina, S.; Das, T.; Haralds, J. T.; Rehr, J. J.; Balatsky, A. V. *Nano Lett.* **2012**, *12*, 927−931.
(24) Sowerby, S. J.; Edelwirth, M.; Heckl, W. M. *J. Phys. Chem. B* **1998**, *102*, 5914−5922.
(25) Mu, Z.; Rubner, O.; Bamler, M.; Blömker, T.; Kehr, G.; Erker, G.; Heuer, A.; Fuchs, H.; Chi, L. *Langmuir* **2013**, *29*, 10737−10743.
(26) Vázquez-Campos, S.; Peter, M.; Dong, M.; Xu, S.; Xu, W.; Gersen, H.; Linderoth, T. R.; Schonherr, H.; Besenbacher, F.; Crego-Calama, M.; Reinhoudt, D. N. *Langmuir* **2007**, *23*, 10294−10298.
(27) Heckl, W. M.; Smith, D. P. E.; Binnig, G.; Klagges, H.; Hansch, T. W.; Maddocks, J. *Proc. Natl. Acad. Sci. U.S.A.* **1991**, *88*, 8003−8005.
(28) Lin, Q.; Zou, X.; Zhou, G.; Liu, R.; Wu, J.; Li, J.; Duan, W. *Phys. Chem. Chem. Phys.* **2011**, *13*, 12225−12230.
(29) Ding, N.; Chen, X.; Wu, C.-M. L.; Li, H. *Phys. Chem. Chem. Phys.* **2013**, *15*, 10767−10776.
(30) Piana, S.; Bilic, A. *J. Phys. Chem. B* **2006**, *110*, 23467−23471.
(31) Levicky, R.; Herne, T. M.; Michael, H.; Tarlov, J.; Satija, S. K. *J. Am. Chem. Soc.* **1998**, *120*, 9787−9792.
(32) Tanaka, H.; Kawai, T. *Mater. Sci. Eng. C* **1995**, *3*, 143−148.
(33) Kumar, A. M. S.; Fox, J. D.; Buerkle, L. E.; Marchant, R. E.; Rowan, S. J. *Langmuir* **2009**, *25*, 653−656.
(34) Reuven, D. G.; Shashikala, H. B. M.; Mandal, S.; Williams, M. N. V.; Chaudhary, J.; Wang, X.-Q. *J. Mater. Chem. B* **2013**, *1*, 3926−3931.
(35) Chiorcea, A.-M.; Oliveira-Brett, A. M. *Bioelectrochemistry* **2002**, *55*, 63−65.
(36) Freund, J. E.; Edelwirth, M.; Krobel, P.; Heckl, W. M. *Phys. Rev. B* **1997**, *55*, 5394−5397.
(37) Choi, S.; Lee, H.; Ghaffari, R.; Hyeon, T.; Kim, D.-H. *Adv. Mater.* **2016**, *28*, 4203−4218.
(38) Saikia, N.; Karna, S. P.; Pandey, R. *Phys. Chem. Chem. Phys.* **2017**, 16819−16830.
(39) Mark, P.; Nilsson, L. *J. Phys. Chem. A* **2001**, *105*, 9954−9960.
(40) Lee, J.-H.; Choi, Y.-K.; Kim, H.-J.; Scheicher, R. H.; Cho, J.-H. *J. Phys. Chem. C* **2013**, *117*, 13435−13441.
(41) Rochefort, A.; Wuest, J. D. *Langmuir* **2009**, *25*, 210−215.
(42) Ng, S. P.; Qiu, G.; Ding, N.; Lu, X.; Wu, C. L. *Biosens. Bioelectron.* **2017**, *89*, 468−476.
(43) Luo, H.; Li, H.; Fu, Q.; Chu, Y.; Cao, X.; Sun, C.; Yuan, X.; Liu, L. *Nanotechnology* **2013**, *24*, No. 495702.
(44) Furlan, S.; Giannozzi, P. *Phys. Chem. Chem. Phys.* **2013**, *15*, 15896−15904.
(45) Tao, N. J.; De Rose, J. A.; Lindsay, S. M. *J. Phys. Chem.* **1993**, *97*, 910−919.
(46) Rosa, M.; Corni, S.; Felice, R. D. *J. Chem. Theory Comput.* **2014**, *10*, 1707−1716.
(47) Phillips, J. C.; Braun, R.; Wang, W.; Gumbart, J.; Tajkhorshid, E.; Villia, E.; Chipot, C.; Skeel, R. D.; Kale, L.; Schulten, K. *J. Comput. Chem.* **2005**, *26*, 1781−1802.
(48) Kang, Y.; Wang, Q.; Liu, Y.-C.; Shen, J.-W.; Wu, T. *J. Phys. Chem. B* **2010**, *114*, 2869−2875.
(49) Deshmukh, S. A.; Kamath, G.; Sankaranarayanan, S. K. R. S. *Soft Matter* **2014**, *10*, 4067−4083.
(50) Darden, T.; York, D.; Pedersen, L. *J. Chem. Phys.* **1993**, *98*, 10089−10092.
(51) Zhao, X. *J. Phys. Chem. C* **2011**, *115*, 6181−6189.
(52) MacKerell, A. D., Jr.; Bashford, D.; Bellott, M., Jr.; Dunbrack, R. L.; Evanseck, J. D.; Field, M. J.; Fischer, S.; Gao, J.; Guo, H.; Ha, S.; Joseph-McCarthy, D.; Kuchnir, L.; Kuczera, K.; Lau, F. T. K.; Mattos, C.; Michnick, S.; Ngo, T.; Nguyen, D. T.; Prodhom, B.; Reiher, W. E., III; Roux, B.; Schlenkrich, M.; Smith, J. C.; Stote, R.; Straub, J.; Watanabe, M.; Wiorkiewicz-Kuczera, J.; Yin, D.; Karplus, M. *J. Phys. Chem. B* **1998**, *102*, 3586−3616.

DOI: 10.1021/acsomega.7b00528
ACS Omega 2017, 2, 3457−3466